



Reduced surface fine dust under droughts over the southeastern United States during summertime: observations and CMIP6 model simulations

Wei Li¹ and Yuxuan Wang¹

¹Department of Earth and Atmospheric Sciences, University of Houston, Houston, Texas, USA.

Corresponding author: Yuxuan Wang (ywang246@central.uh.edu)

Abstract. Drought is an extreme hydroclimate event that has been shown to cause the increase of surface fine dust near source regions, while the drought-dust relationship in regions predominantly influenced by long-range transported dust such as the southeastern US (SEUS) has received less attention. Using long-term surface fine dust observations, weekly US Drought Monitor (USDM), and monthly Standardized Precipitation-Evapotranspiration Index (SPEI), this study unmasks spatial disparity in drought-dust relationships where the SEUS stands out as being abnormal in that it shows a decrease in surface dust concentrations during drought in contrast to the expected increase in dust found in other contiguous US (CONUS) regions. Surface fine dust was found to decrease by $\sim 0.5 \mu\text{g}/\text{m}^3$ with a unit decrease of SPEI in the SEUS, as opposed to an increase of $\sim 0.15 \mu\text{g}/\text{m}^3$ in the west. The anomalies of elemental ratios, satellite aerosol optical depth (AOD), and dust extinction coefficients suggest that both the emissions and trans-Atlantic transport of African dust are weakened when the SEUS is under droughts. Through the teleconnection patterns of negative North Atlantic Oscillation (NAO), a lower than normal and more northeastward displacement of the Bermuda High (BH) was present during SEUS droughts which resulted in less dust being transported into the SEUS. At the same time, enhanced precipitation in Sahel associated with the northward shift of the Intertropical Convergence Zone (ITCZ) leads to lower dust emissions therein. Of the four selected models participating in the sixth phase of the Coupled Model Intercomparison Project (CMIP6), GISS-E2-1-G was found to perform the best in capturing the drought-dust sensitivity in the SEUS. This study reveals the mechanism of how regional-scale droughts influence aerosol abundance through changing long-range transport of dust.



28 **1 Introduction**

29 Mineral dust plays an important role in the climate system by modifying the Earth's energy budget through direct
 30 aerosol-radiation forcing and indirect aerosol-cloud interactions (Tegen et al., 1996; Sassen, 2002; Carslaw et al.,
 31 2010). Fine mode mineral dust with an aerodynamic diameter of less than 2.5 μm can be transported over long
 32 distances and has a wide-ranging socioeconomic effect such as degeneration of air quality, disruption of public
 33 transport by poor visibility, and reduction of soil productivity (Middleton, 2017). Dust events can also be linked with
 34 a higher risk of valley fever and other respiratory and cardiovascular diseases (Karanasiou et al., 2012; Tong et al.,
 35 2017), and more non-accidental mortality (Crooks et al., 2016). Lifted by strong winds from arid and bare land, dust
 36 particles in the atmosphere are significantly modulated by hydroclimate variables, such as precipitation, temperature,
 37 relative humidity, and soil moisture (Achakulwisut et al., 2017; Brey et al., 2020; Pu and Ginoux, 2018). Thus,
 38 drought, as a recurring hydroclimate extreme, can impose large changes on the abundance of dust particles in the
 39 atmosphere. As the contiguous United States (CONUS) is prone to droughts and projected to be warmer and dryer in
 40 the future (Cook et al., 2015), it is essential to quantify the drought-dust relations and evaluate the ability of climate
 41 models to capture such relations to better understand the climate-dust feedbacks.

42 Most of the previous studies of drought-dust sensitivity in the US focused on the southwest (Aarons et al., 2019;
 43 Achakulwisut et al., 2018, 2019; Arcusa et al., 2020; Borlina and Rennó, 2017; Kim et al., 2021) where the major dust
 44 emission sources are located (e.g. the Chihuahuan, Mojave, and Sonoran Deserts). For example, Achakulwisut et al.
 45 (2018) quantified an increase of fine dust by 0.22–0.43 $\mu\text{g}/\text{m}^3$ with a unit decrease of two-month Standardized
 46 Precipitation-Evapotranspiration Index (SPEI) over the US southwest across the seasons. Both observations (Aarons
 47 et al., 2019) and simulations (Kim et al., 2021) have shown that the dust enhancement under droughts can be attributed
 48 to the simultaneous increase of local dust emissions and long-range transport of dust from Asia. The observed drought-
 49 dust relationship can be used as a process-level metric to evaluate dust simulation in coupled chemistry-climate models
 50 and Earth system models. For example, a recent evaluation of dust emissions in 19 models participating in the sixth
 51 phase of the Coupled Model Intercomparison Project (CMIP6) found that interannual variations of dust emissions
 52 simulated by these models are strongly correlated with drought over major dust source regions (Aryal and Evans,
 53 2021).

54 While the abovementioned studies improved our understanding of dust-drought relationships in dust source areas,
 55 regions predominantly influenced by long-range transported dust such as the southeastern US (SEUS) have received
 56 less attention. The dusty Saharan air from western Africa can reach the US southeast during boreal summer through
 57 long-range transport across the tropical Atlantic Ocean and Caribbean Basin (e.g., Perry et al., 1997; Prospero et al.,
 58 2010). Fine dust is estimated to contribute to 20–30% of the total particulate matter smaller than 2.5 μm (PM_{2.5})
 59 aerodynamic diameter at the surface in the southeast during summertime (Hand et al., 2017). Extreme “Godzilla” dust
 60 events have occurred in recent years, leading to considerably worse air quality in the southeast region (Yu et al., 2021).
 61 Our previous study (Wang et al. (2017) estimated that growing-season (March–October) droughts during 1990–2014
 62 caused an average fine dust increase of 27% in the west and 16% in the Great Plains, with a much lower effect on fine



63 dust in the southeastern and northeastern US. That study used a coarse time scale (i.e., averaging of the eight-month
 64 growing season) which may not fully capture the episodic nature of dust emissions or dust transport.

65 Here we improve upon previous studies by using drought and dust datasets of better spatial coverage and finer
 66 temporal scales (Section 2). In Section 3.1, we first examine how the spatial distributions of surface fine dust change
 67 with weekly and monthly drought indices over the CONUS. The finer-scale analysis unmasks spatial disparity in
 68 drought-dust relationships where the SEUS stands out as being abnormal in that it shows a decrease in surface dust
 69 concentrations during drought in contrast to the expected increase in dust found in other CONUS regions. We then
 70 focus on the southeast, an area largely overlooked by prior studies of dust response to drought, and investigate in
 71 Section 3.2 how drought conditions in the SEUS affect the trans-Atlantic transport of African dust.

72 Among the surface fine dust measurement datasets examined in this study, the Barbados site located in the eastmost
 73 of the Caribbean Windward Islands is the only long-term site on the main outflow pathway of African dust to the
 74 SEUS, which is suitable to evaluate dust-drought relationships simulated by coupled climate-chemistry models. The
 75 surface dust mass concentration has been continuously measured at the Barbados site since August 1965. This rare
 76 and unique dataset was widely used to improve our understanding of the variations of African dust transport and model
 77 evaluations (Chiapello et al., 2005; Prospero and Nees, 1986; Zuidema et al., 2019). Given the correct sensitivity of
 78 dust emissions to drought in CMIP6 models (Aryal & Evans, 2021), in Section 3.3 we use the dust-drought relationship
 79 at the Barbados site to evaluate the performance of four CMIP6 models in capturing the drought-dust sensitivity in
 80 the SEUS.

81 **2 Data and Methods**

82 The datasets and related variables used in this study were summarized in Table S1-2 with details given below.

83 **2.1 Drought indicator**

84 The US Drought Monitor (USDM) index was selected as the primary drought indicator because it incorporates not
 85 only objective indicators but also inputs from regional and local experts around the country (Svoboda et al., 2002).
 86 USDM maps have been released every week from 2000 to the present on its website (<https://droughtmonitor.unl.edu/>).
 87 There are five dryness categories in the map, labeled Abnormally Dry (D0), Moderate (D1), Severe (D2), Extreme
 88 (D3), and Exceptional (D4) Drought. We converted these maps into $0.5^\circ \times 0.5^\circ$ gridded data and combined D2-D4
 89 levels as “severe drought” due to limited data availability caused by their low spatial coverage if treated individually
 90 (Li et al., 2022). Non-drought (wet and normal) conditions, denoted as N0, are defined when a grid is not under any
 91 of the five dryness categories. There are 262 weeks in total during our study period of 2000 to 2019 summers (June,
 92 July, August; JJA). To compensate for the categorical nature of the USDM data, one-month gridded SPEI data from
 93 the global SPEI database (<http://sac.csic.es/spei/>) with a spatial resolution of $0.5^\circ \times 0.5^\circ$ and temporal range of 1973-
 94 2018 was also used to conduct statistical analysis (e.g., correlation and regression). The criteria of $\text{SPEI} < -1.3$ and



95 SPEI > -0.5 were applied to denote severe drought and non-drought conditions, respectively, as suggested by Wang
 96 et al. (2017).

97 **2.2 Surface dust and satellite products**

98 To expand the spatial coverage, we created a gridded daily fine dust dataset ($1^\circ \times 1^\circ$) that aggregates site-based
 99 observations from both US Environmental Protection Agency Chemical Speciation Network (EPA-CSN) and the
 100 Interagency Monitoring of Protected Visual Environments (IMPROVE) networks using the modified inverse distance
 101 weighting method as done by Schnell et al., (2014). These two datasets have been widely used by previous studies to
 102 investigate surface fine dust variations (Achakulwisut et al., 2017; Hand et al., 2017; Kim et al., 2021). The gridded
 103 dust data was further remapped through bilinear interpolation to match the spatial resolution of the USDM and SPEI
 104 data. We used the latest version of total surface dust data at the Barbados site (Figure 4b) created and published by
 105 Zuidema et al. (2019). The Barbados JJA monthly data was averaged from at least 20 daily samples in each month
 106 between 1973 and 2014.

107 To examine the westward transport of African dust, Level3 daily aerosol optical depth AOD (550nm) retrieved from
 108 Moderate Resolution Imaging Spectroradiometer (MODIS) aboard Aqua (MYD07_D3 v6.1) and Terra (MOD08_D3
 109 v6.1) with a resolution of $1^\circ \times 1^\circ$ from 2003 to 2019 are combined (Payra et al., 2021; Pu and Jin, 2021). Level3
 110 monthly cloud-free dust extinction coefficients at 532nm between 2006 and 2019 from Cloud-Aerosol Lidar and
 111 Infrared Pathfinder Satellite Observation (CALIPSO) satellite were also used to analyze the vertical profiles of trans-
 112 Atlantic dust plumes. The CALIPSO data was obtained from <https://asdc.larc.nasa.gov/project/CALIPSO> with a $2^\circ \times$
 113 5° horizontal grid and a vertical resolution of 60 m up to 12km from the ground.

114 **2.3 Meteorological data**

115 To analyze the emission and transport of African dust, several meteorological variables were applied. Daily
 116 precipitation was taken from the Global Precipitation Climatology Project version 1.3 (GPCP V1.3). The data is a
 117 satellite-based global product from 1996 with a $1^\circ \times 1^\circ$ spatial resolution. Other variables, including zonal (U) and
 118 meridional (V) winds, and geopotential height at different pressure levels were from the European Centre for Medium
 119 Range Weather Forecast (ECMWF) reanalysis version5 (ERA5) dataset. Weekly data was averaged from hourly data
 120 with a resolution of $0.25^\circ \times 0.25^\circ$. Monthly North Atlantic Oscillation (NAO) data was obtained from the Climate
 121 Research Unit (CRU) calculated as the difference of normalized sea-level pressure between Azores and Iceland (Jones
 122 et al., 1997).

123 **2.4 CMIP6 models**

124 Four models from the CMIP6 Aerosol Chemistry Model Intercomparison Project (AerChemMIP) were selected:
 125 CNRM-ESM2-1, GFDL-ESM4, GISS-E2-1-G, and MRI-ESM2-0. They are the only models found with surface dust
 126 outputs from historical simulations with prescribed sea surface temperature. All the model outputs cover the period of
 127 1850 to 2014. Dust emissions are interactively calculated based on factors such as surface wind speed, soil type, and



128 aridity. Dust particles are resolved to different size bins ranging from 0.01 to 32 μm in diameter. More information
 129 and references (Dunne et al., 2020; Kelley et al., 2020; Séférian et al., 2019; Yukimoto et al., 2019) for each model
 130 are listed in Table S2.

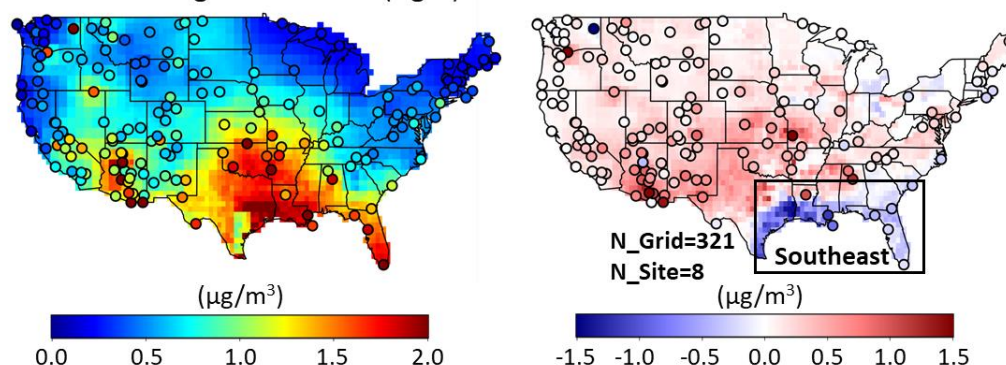
131 **3 Results**

132 **3.1 Reduced dust in the southeast under droughts**

133 Figure 1a shows the mean summertime (JJA 2000 – 2019) surface fine dust concentrations under non-drought
 134 conditions (N0) and their changes under severe droughts (D2-D4) relative to non-drought. Higher concentrations (~ 2
 135 $\mu\text{g}/\text{m}^3$) can be found in the southwest and southeast regions under non-drought conditions, reflecting the average
 136 spatial distributions of summertime dust. Under severe droughts, most of the grids/sites display an enhanced dust
 137 level, with the highest enhancement ($\sim 1.5 \mu\text{g}/\text{m}^3$) occurring near the source regions in the southwest (e.g., Arizona
 138 and New Mexico). This indicates higher local dust emissions under droughts, which can be attributable to regional
 139 precipitation, bareness, wind speed, and soil moisture anomalies (Achakulwisut et al., 2017; Kim et al., 2021; Pu and
 140 Ginoux, 2018). By contrast, reduced fine dust is shown in the southeastern grids/sites under severe drought, especially
 141 for the ones near the coast. Density plots in Figure 1b illustrate that the overall gridded dust distributions under severe
 142 droughts across the CONUS move towards the high end compared with non-drought conditions, with an increase of
 143 the mode and mean value by $\sim 0.12 \mu\text{g}/\text{m}^3$ and $\sim 0.20 \mu\text{g}/\text{m}^3$, respectively. Conversely, dust distributions over the
 144 southeast ($25^\circ\text{--}33^\circ\text{N}$, $100^\circ\text{--}75^\circ\text{W}$; black box in Figure 1a) move to the low end with a respective decrease of the mode
 145 and mean value by $\sim 0.41 \mu\text{g}/\text{m}^3$ and $\sim 0.23 \mu\text{g}/\text{m}^3$. To test whether the spatial interpolation process could potentially
 146 cause bias due to the low site numbers over the southeast region, Figure 1b also plots the density distribution using
 147 on-site IMPROVE data. Similar distributions can be seen between the gridded and on-site data, except that the latter
 148 shows a “fatter” (more variable) distribution. This indicates that the interpolation did not significantly affect the
 149 results.



(a) Dust distribution under non-drought conditions (left) and its changes from severe drought conditions (right)



(b) Dust density plot over the CONUS (left) and the southeast region (right)

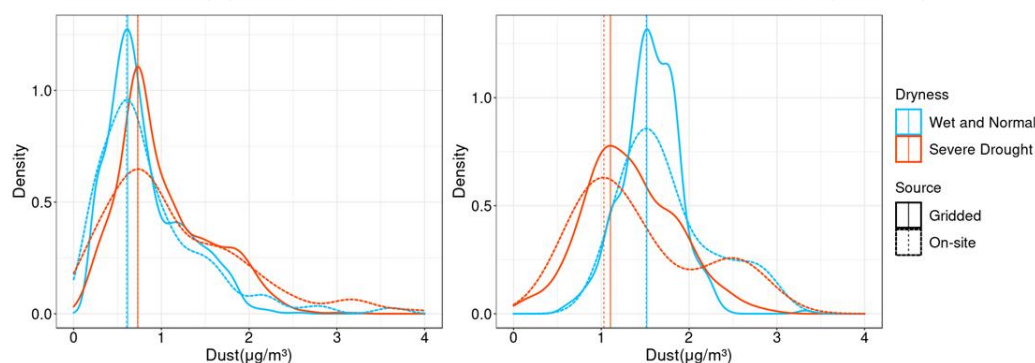
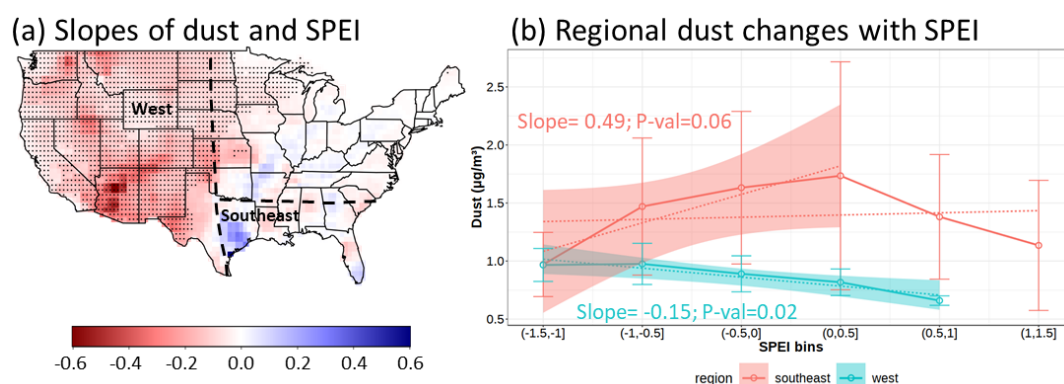


Figure 1. (a) Maps of the mean gridded and in-situ (dots) fine dust under USDM-based non-drought (wet and normal) conditions (left) from 2000 to 2019 and its changes from severe drought conditions (right). The number of grids (sites) within the southeast region is denoted by N_Grid (N_Site). (b) Comparisons of density distributions of gridded (solid lines) and in-situ (dash lines) fine dust concentrations under drought (red lines) and non-drought (blue lines) conditions over the CONUS (left) and southeast region (right), respectively. Vertical dash and solid lines indicate the modes.

We also reproduced the above analysis using SPEI-based monthly drought criteria and similar results were found (Figure S1). The consistency indicates the drought-dust relationship can be captured on both a weekly and monthly scale. To further quantify the drought-dust relationship, we conducted a linear regression between SPEI and dust concentrations, taking advantage of the non-categorical nature of SPEI. The slopes of the regression at each grid were shown in Figure 2a. Almost all the grids in the western CONUS have significant negative slopes at a 95% confidence level. As negative SPEI values indicate drought, these negative slopes reveal an increasing level of dust with dryer conditions. The highest value about $-0.6 \mu\text{g}/\text{m}^3$ per SPEI unit occurs in Arizona, which is also indicative of higher dust emissions consistent with the composite analysis in Figure 1. However, not all the grids in the southeast exhibit significant positive slopes as expected from Figure 1. This may imply a non-linear relationship that cannot be identified via composite analysis. To better explain this, we compared how the regional mean dust concentrations vary with SPEI bins between the southeast (same as Figure 1) and west (100°W westwards) in Figure 2b. A clear nonlinear



167 pattern is revealed for the southeast with dust decreasing with the absolute value of SPEI in both wet (SPEI > 0.5) and
 168 dry (SPEI < -0.5) portions. By contrast, the west exhibits a linear relationship throughout the SPEI range. Decreasing
 169 dust conditions with increasing wetness (SPEI > 0) is expected as dust in the atmosphere can be largely washed out
 170 by precipitation under wet conditions. However, including SPEI bins larger than zero would result in a near-zero slope
 171 from the linear regression in the southeast. To avoid this, we conducted the linear regression using only the lowest
 172 four SPEI bins under dry conditions (SPEI < 0.5). The resulting regression slope is $0.49 \mu\text{g}/\text{m}^3$ per unit of SPEI for
 173 the southeast and $-0.15 \mu\text{g}/\text{m}^3$ per unit of SPEI for the west, respectively. As SPEI is more negative with increasing
 174 dryness, the positive slope in the southeast means a decrease of dust with increasing dryness which is consistent with
 175 the result from Figure 1 based on USDM. Hereafter we focused on the southeast region and investigated why surface
 176 fine dust in this region shows an opposite response to droughts compared with other CONUS regions.



177

178 **Figure 2. (a) Maps of the linear regression slopes between fine dust concentrations and SPEI. Black dots denote the grids**
 179 **with regression significance at a 95% confidence level. Dash lines mark the boundaries of the west and southeast regions.**
 180 **(b) Regional average dust varies with SPEI bins over the west and southeast with error bars indicating one standard**
 181 **deviation. Dash lines display linear regression results with shadings showing the 95% confidence level. The numbers**
 182 **indicate the slopes and P-values (P-val) of the regression using all the SPEI bins in the west and only the first four bins**
 183 **in the southeast.**

184 Dust elemental ratios contain important information signifying the dust particle origins (e.g., local or transport).
 185 African dust, relative to Asian and local dust, normally has higher Fe:Ca (> 1.50) and Al:Ca (> 2.60) ratios, and lower
 186 K:Fe (< 1.10) and Si:Al (< 2.90) ratios (Aldhaif et al., 2020; Gonzalez et al., 2021; VanCuren and Cahill, 2002). Based
 187 on these reported thresholds, we analyzed dust elemental observations at eight sites within the southeast region (Figure
 188 1a) and compared how the elemental ratios changed under severe drought based on the USDM drought indicator. The
 189 results are displayed in Figure 3, with more statistical descriptions listed in Table S3. Under non-drought conditions
 190 (wet and normal), the ratios are generally within the typical ranges mentioned above, indicating the dominance of
 191 African dust over Asian dust and locally-emitted dust as reported by other studies (Aldhaif et al., 2020; VanCuren and
 192 Cahill, 2002). Under severe drought, Fe:Ca and Al:Ca become lower; K:Fe and Si:Al become higher, and all these
 193 changes are in the direction of reducing the characteristic elemental ratios of African dust. Most of the Fe:Ca, Al:Ca,
 194 and K:Fe ratios under severe drought have their medians falling below the reported thresholds of African dust. This



indicates a significantly reduced dust source from Africa. As dust deposition is unlikely to increase under drought conditions, the lower African dust signature in surface dust under severe drought is most likely attributable to the reduced import of African dust to the SEUS, which is discussed below.

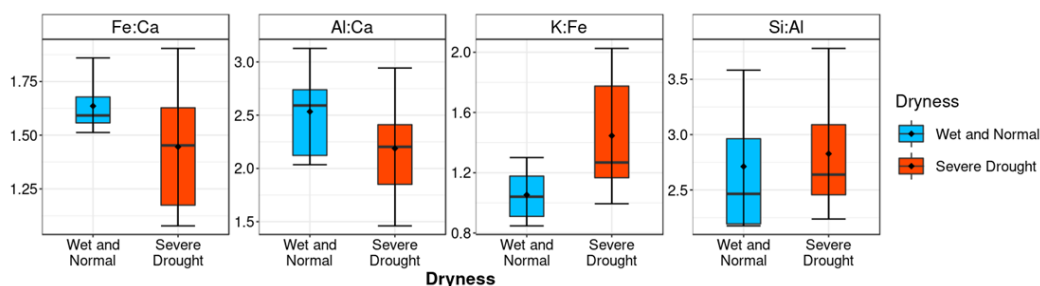


Figure 3. Boxplots of four dust elemental ratios under non-drought (wet and normal) and severe drought conditions. Observations are from eight IMPROVE sites in the southeast region shown in Figure 1a. The upper and lower whiskers of the boxplots represent the ninth and first quantile, respectively. Black dots indicate the mean values. Detailed values of this figure can be found in Table S3.

3.2 Weakened trans-Atlantic dust transport under droughts

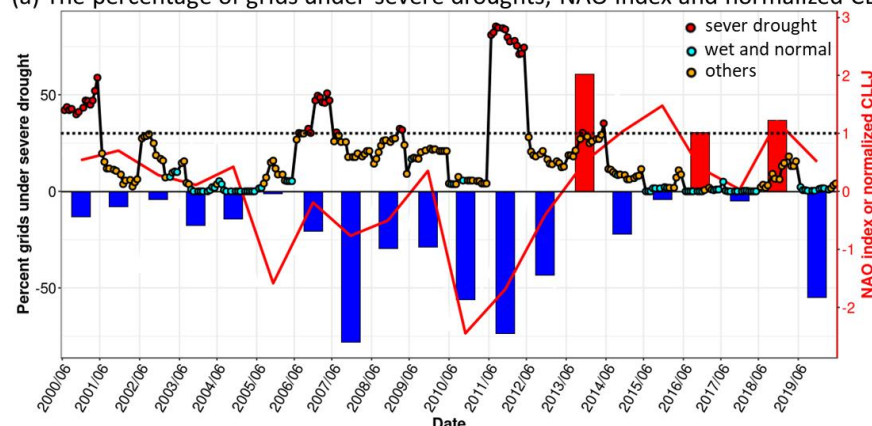
In this section, we examined how the trans-Atlantic transport of African dust changes with droughts in the southeast region. To do so, we first selected regional-scale drought events to better depict the aridness across the southeast, and then associated these events with the long-range transport of African dust and compared them with regional-scale non-drought events. Regional severe drought (non-drought) events were identified when more than 30% (70%) of the southeastern grids are under D2-D4 (N0) on a weekly scale (USDM-based), or when the regional-mean SPEI is within (out of) the lowest 20% percentile during the study period (dependent on data records) on a monthly scale (SPEI-based). The time series in Figure 4a shows that the regional drought events mainly occurred in 2000, 2006, 2007, and 2011 JJA.

Maps of MODIS AOD under non-drought conditions and its changes during severe droughts are shown in Figure 4b. Horizontally, the major transport pathway of the dusty African air is within 10°-20°N, 100°-0°W (red box), indicated by the high AOD values greater than 0.15. The dust flow, emitted from northern Africa (e.g., Sahara Desert and Sahel), travels through the tropical Atlantic, Caribbean Sea, Gulf of Mexico and reaches the SEUS. Under droughts, almost all the AOD values along the pathway show negative differences, which indicates both the African dust transport and emissions (mainly from the Sahel) are depressed when the SEUS is under droughts. To better present the transport pathway, we also examined the vertical profiles of the dust extinction coefficient from CALIPSO along the pathway (Figure 4c). Since the CALIPSO data is monthly, we used the SPEI-based drought events definition here. The dust particles can be injected up to ~4km altitude from the source region through strong desert surface heating (Alamirew et al., 2018; Flamant et al., 2007), low-level wind convergence (Bou Karam et al., 2008), synoptic-scale disturbance (Knippertz and Todd, 2010) and other processes (Francis et al., 2020), and then descend to lower levels as they travel westwards. Such vertical structures have been discerned by previous studies (Prospero and Mayol-Bracero, 2013;

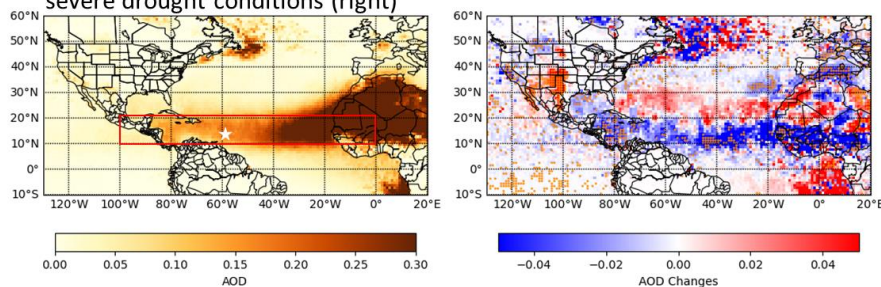


224 Ridley et al., 2012). Similar to Figure 4b, a decreased dust extinction coefficient was found along the vertical transport
 225 pathway, which verifies the conclusion that both the transport and emissions of African dust are weakened when the
 226 SEUS is under droughts.

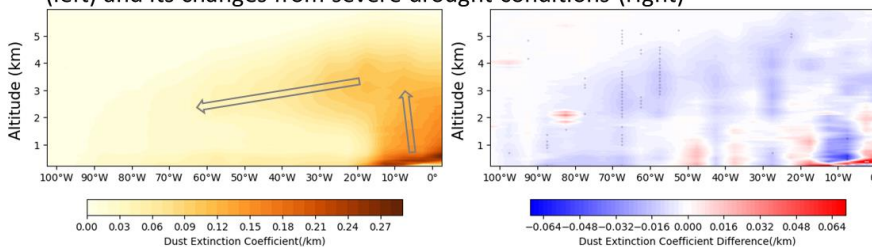
(a) The percentage of grids under severe droughts, NAO index and normalized CLLJ



(b) MODIS AOD under wet and normal conditions (left) and its changes from severe drought conditions (right)



(c) Dust extinction coefficient vertical profile under wet and normal conditions (left) and its changes from severe drought conditions (right)

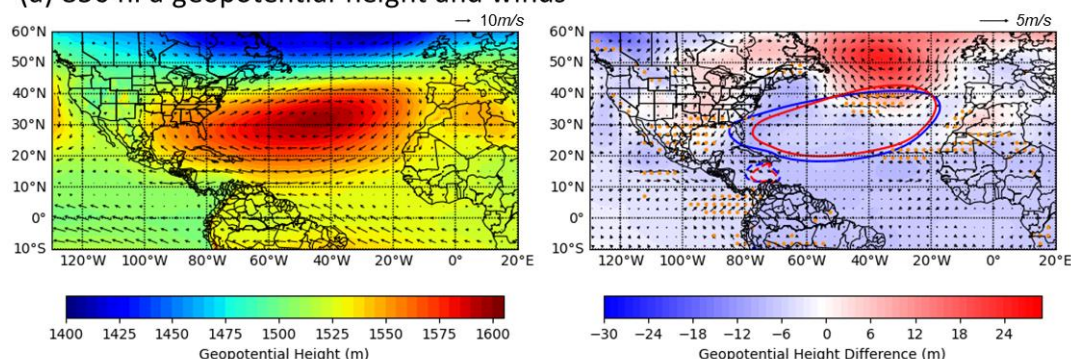


227

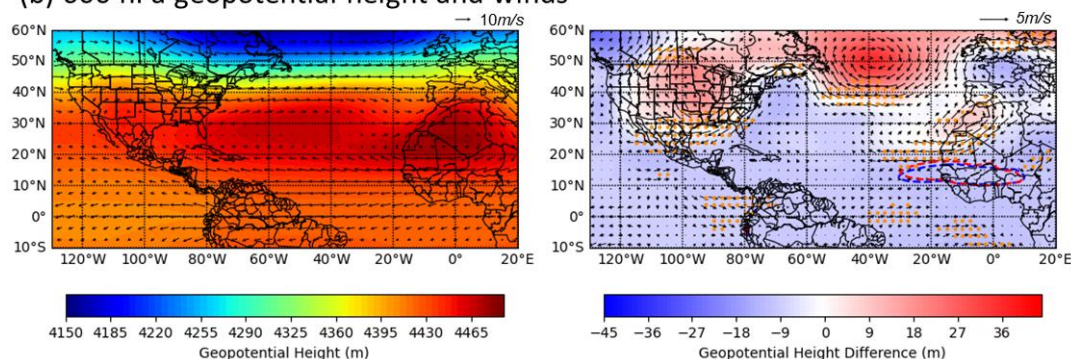
228 **Figure 4.** (a) Time series of weekly regional dryness levels indicated by the percentage of grids under severe drought (D2-
 229 D4) in the southeast area (filled dots; left axis), the JJA-mean North Atlantic Oscillation (NAO) index (bars; right axis) and
 230 normalized Carrabin low-level jet (CLLJ) (red line; right axis). The black dash line indicates the position of 30%. (b) Maps
 231 of AOD under non-drought (wet and normal) conditions (left column) and its changes from severe droughts (right column)
 232 based on the weekly time series in a. The white asterisk denotes the location of the Barbados site (13°6'N, 59°37'W). (c) The
 233 same as b except for showing the vertical profiles of dust extinction coefficient over the major transport pathway (red box
 234 in b) based on monthly SPEI between 2006 and 2018. Black or orange dots in b and c (right column) indicate the significant
 235 difference at a 95% confidence level relative to non-drought conditions.



(a) 850 hPa geopotential height and winds



(b) 600 hPa geopotential height and winds



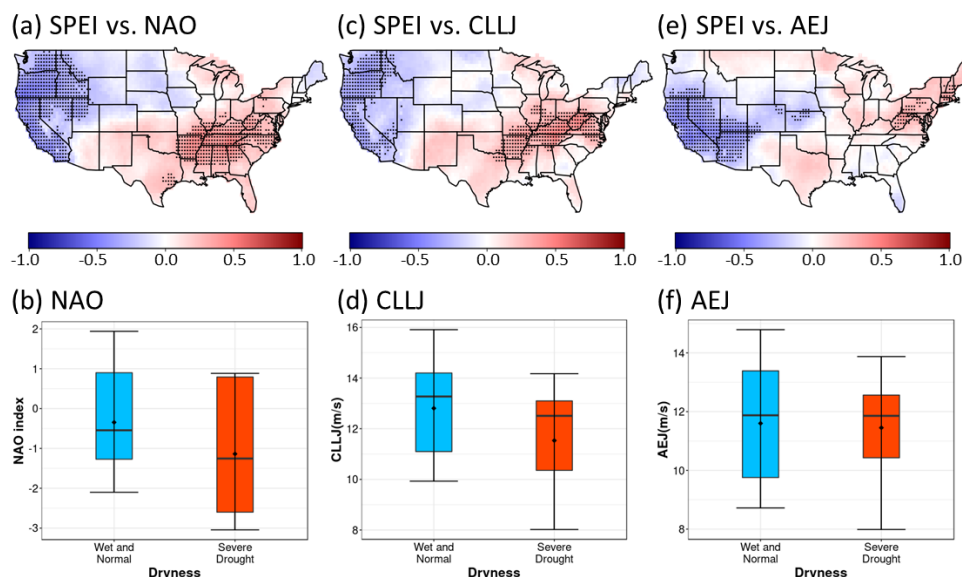
236

237 **Figure 5. Maps of geopotential height (shadings) and wind vectors (arrows) at 850 hPa (a) and 600 hPa (b) under USDM-**
 238 **based non-drought (wet and normal) conditions (left column) and their changes during severe drought periods (right**
 239 **column). Solid lines in a indicate the edge of Bermuda High under non-drought (blue) and severe droughts (red). Dash lines**
 240 **show the edge of Caribbean low-level jet (a) and African easterly jet (b) under non-drought (blue) and severe droughts**
 241 **(red). Orange dots (right column) indicate the grids with significant differences of zonal winds at a 95% confidence level.**

242 The teleconnections between the SEUS droughts and the transport and emissions of African dust are displayed in
 243 Figure 5. At low levels near the central North Atlantic, a semipermanent high-pressure system called North Atlantic
 244 Subtropical High (NASH) or Bermuda High (BH) favors the dust transport with its southwestward extensions towards
 245 the Caribbean and Gulf of Mexico steering dust into CONUS (Doherty et al., 2008; Kelly and Mapes, 2011). This can
 246 be clearly seen from the anticyclonic wind circulations in Figure 5a. Using the 1560m contour (solid lines in Figure
 247 5a) as the edge of the BH following Li et al. (2011), a retreat of the BH towards the northeast can be recognized under
 248 droughts, causing northerly wind anomalies over the Caribbean and Gulf of Mexico. As the normal winds are
 249 southerly, the northerly wind anomalies reveal a weakened dust transport into the SEUS. Accompanied by the
 250 southwestward extension of BH, the Caribbean low-level jet (CLLJ), defined as the mean zonal wind speed at 925
 251 hPa over 11°–17°N, 70°–80°W, is also used to assess the westward transport of dust over the Caribbean Sea (Wang,
 252 2007). The edge of CLLJ is denoted by the 12 m/s zonal wind speed contour (dash lines in Figure 5a). The shrinkage
 253 of CLLJ under droughts further verifies the weakened dust transport at low levels.



254 The geopotential height pattern associated with these circulation and jet changes is a higher than normal subpolar low
 255 and lower than normal BH, which is consistent with the negative phase of North Atlantic Oscillation (NAO) (Barnston
 256 and Livezey, 1987). A negative phase of NAO has been proven to be teleconnected with dry weather over the SEUS
 257 and northern Europe, and wet weather over southern Europe and the Mediterranean due to fewer and weaker storms
 258 caused by the reduced pressure gradient between the subtropical high and low (Hurrell, 1995; Visbeck et al., 2001).
 259 The time series in Figure 4a show severe drought events (e.g., 2011) are associated with strong negative NAO and
 260 abnormally low CLLJ. Similarly, we found both NAO and CLLJ are positively correlated with SPEI over the SEUS
 261 (Figure 6a, c) with their corresponding mean magnitude reduced by 0.80 and 1.27 m/s compared with non-drought
 262 conditions (Figure 6b, d). This further confirms the weakened low-level dust transport into the southeast region.



263

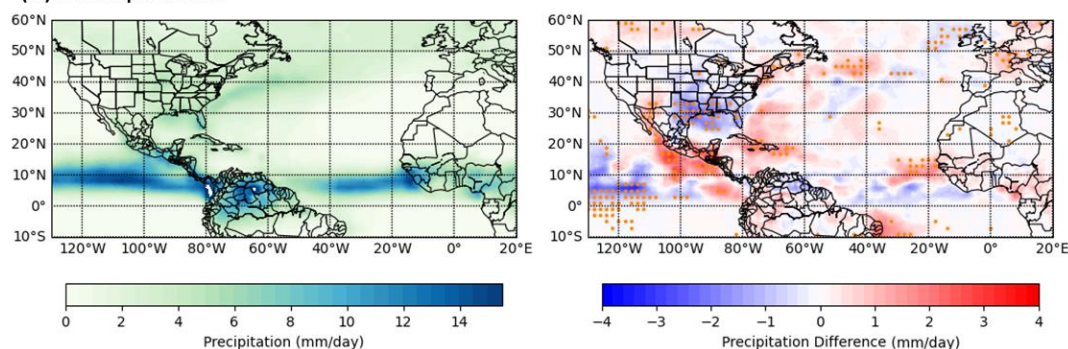
264 **Figure 6. Map of the correlation coefficient between SPEI and NAO (a), CLLJ (c), and AEJ (e) with black dots denoting**
 265 **the significant correlation at 95% confidence level. And the boxplots of NAO (b), CLLJ (d), and AEJ (f) distributions under**
 266 **non-drought (wet and normal) and severe drought conditions.**

267 The westward dust propagation at high levels (e.g., at ~3 km altitude) mainly occurs near the source region after being
 268 injected from the surface (Figure 4c). The African easterly jet (AEJ), defined as the average zonal wind speed at 600
 269 hPa over the area of 10°–15°N, 30°W–10°E (Cook, 1999), has been widely linked with the transport of the African
 270 dust towards tropical Atlantic (e.g., Jones et al., 2003; Pu & Jin, 2021). Another strengthened high pressure over North
 271 Africa (Saharan Anticyclone) at 600 hPa (also seen at 850 hPa) leads to stronger winds to the northern rim of AEJ
 272 (Figure 5b). However, the core jet area seems to be less affected as shown by the comparable magnitude of AEJ
 273 between non-drought and drought conditions in Figure 6f. The edge of AEJ, denoted by the 11 m/s zonal wind contour
 274 (dash lines in Figure 5b), only slightly moves northwards and does not show noticeable expansion or shrinkage. There
 275 are no significant correlations between SPEI and AEJ over the SEUS either (Figure 6c), which indicates weak

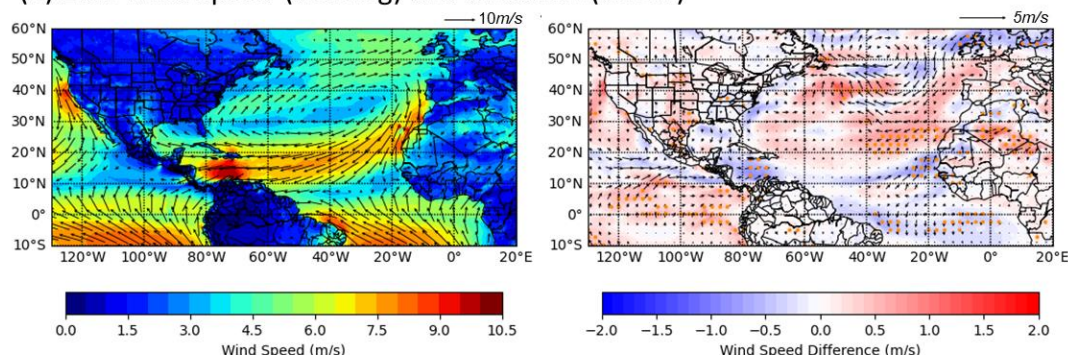


teleconnection exists between droughts in the SEUS and the dust transport strength at a high level. The abnormally high Saharan Anticyclone at both 850 hPa and 600 hPa (Figure 5a-b) is likely to intensify both emissions and transport of dust from the Sahara Desert as seen from the positive differences in Figure 4b.

(a) Precipitation



(b) 10m wind speed (shading) and direction (arrow)



279

280 **Figure 7. Maps of precipitation (a) and 10m wind speed (shadings in b) and directions (arrows in b) under USDM-based**
 281 **non-drought (wet and normal) conditions (left column) and their changes during severe drought periods (right column).**
 282 **Orange dots (right column) indicate the grids with significant differences of precipitation (a) and wind speed (b) at a 95%**
 283 **confidence level.**

284 Precipitation is one of the dominant factors influencing African dust emissions (Moulin and Chiapello, 2004). A
 285 maximum precipitation zonal belt near 5°–10°N can be seen under non-drought conditions in Figure 7a, which
 286 represents the location of the Intertropical Convergence Zone (ITCZ). We found enhanced precipitation in southern
 287 West Africa (10°–20°N, 30°–0°W) and the Caribbean Sea, which will reduce dust emissions from the major source
 288 region of Sahel (e.g., southern Mauritania and Mali) and intensify the wet scavenging of dust to the Caribbean Sea. A
 289 significant anticorrelation between summertime Sahel precipitation and NAO has been reported by previous studies
 290 on a multidecadal scale (Folland et al., 2009; Linderholm et al., 2009) caused by the northward displacement of ITCZ
 291 shifting the “rain belt” into the Sahel region in response to a warmer North Atlantic (Sheen et al., 2017; Yuan et al.,
 292 2018). By locating the maximum rainfall within 0°–20°N, 30°–0°W following Liu et al., (2020), we found an average



293 of $\sim 0.6^\circ$ norward movement of ITCZ during the SEUS droughts. This can also be seen from the southwesterly 10m
 294 wind anomalies over the same region, which are contradicting to the northeasterly winds under non-drought conditions
 295 (Figure 7b). Surface wind speed is another important factor associated with dust emissions in this region (Evan et al.,
 296 2016). However, Figure 7b does not show clear negative anomalies over the Sahel region under droughts, which
 297 implies that surface wind speed is not a significant factor causing the weakened dust emissions in the Sahel.

298 In summary, the reduction of surface fine dust in the SEUS under severe drought results from the weakened African
 299 dust transport and emissions from the Sahel through the teleconnection patterns of negative NAO. The weaker and
 300 less southwestward extension of BH reduces the wind speed over the Caribbean and Gulf of Mexico, making it less
 301 favorable for African dust to enter the SEUS at low levels. Intensified precipitation over Sahel related to the northward
 302 shift of ITCZ is the main factor causing lower Sahelian dust emissions during the SEUS droughts, and this factor
 303 dominates over surface wind speed changes.

304 **3.3 CMIP6 model evaluation**

305 In this section, we evaluated the surface dust concentrations from four CMIP6 models regarding their capability of
 306 capturing the drought-dust relationships in the SEUS in comparison with the monthly observations (1973-2014; JJA)
 307 at the Barbados site. Dust values were extracted at a grid point nearest to the observation site. Out of the 120-month
 308 study period, 24 severe drought months were identified based on the same SPEI-based regional-drought criteria as
 309 described in the last section.

310 Figure 8a displays the scatter plots between model simulations and observations with more statistics listed in Table 1.
 311 CNRM-ESM2-1 considerably underestimates the dust concentrations by more than $20 \mu\text{g}/\text{m}^3$ (80%) regardless of the
 312 drought conditions. This is possibly due to its relatively high dry deposition (Zhao et al., 2021). GFDL-ESM4
 313 simulations have a relatively lower underestimation of $\sim 7 \mu\text{g}/\text{m}^3$ (26%) but do not reproduce the variability as
 314 indicated by the negative correlation coefficient (R) and slope. Under droughts, the underestimation is reduced by
 315 $\sim 50\%$ with R and slope values turning to positive, which indicates this model has better performance under droughts.
 316 An overall overestimation by $4.92 \mu\text{g}/\text{m}^3$ (17.93%) was found in the simulations of GISS-E2-1-G. A near-zero value
 317 of R and slope also show that the GISS-E2-1-G model can barely capture the dust variability. If only the drought
 318 months are considered, GISS-E2-1-G has a better model performance in predicting the dust variability with R
 319 increasing to 0.38. MRI-ESM2-0 generally shows a minimum bias with an underestimation of ~ 4.76 (17.38%), yet a
 320 poor capability of reproducing the dust variability. Using drought months alone does not improve the performance,
 321 implying its dust simulations are not sensitive to drought conditions.

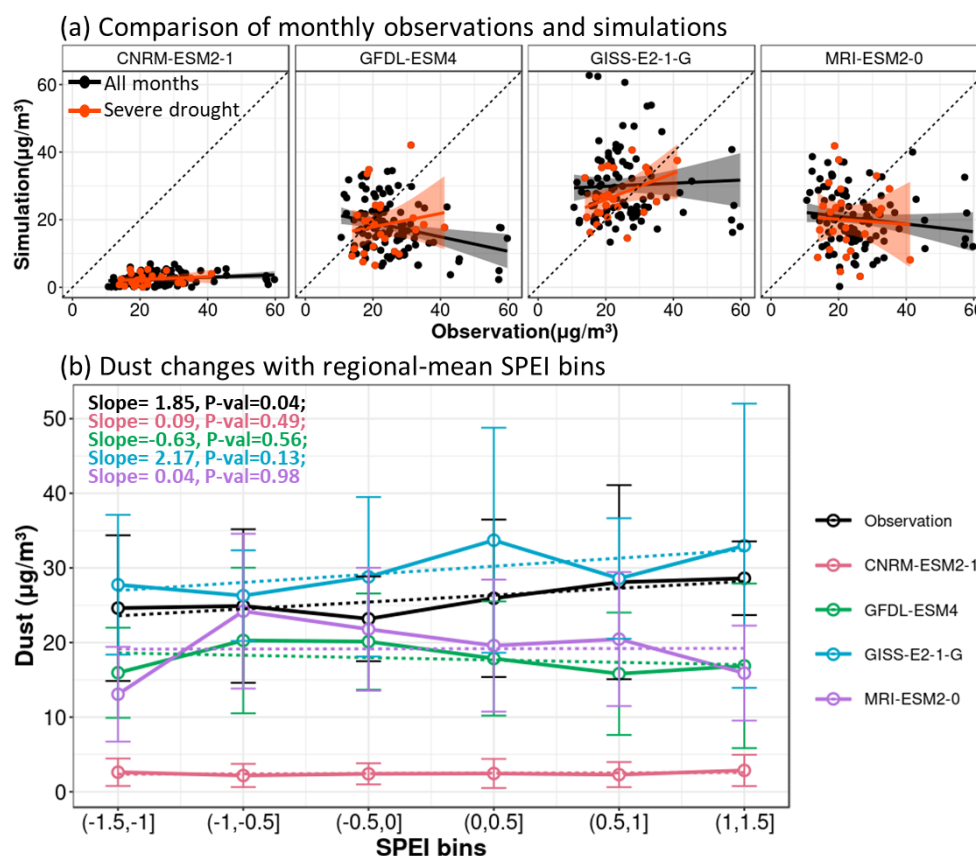


Figure 8. (a) Scatter plots between dust observations and four CMIP6 models. Black (red) dots and lines represent dust in all (severe drought) months and their linear regression fits, respectively. The shadings indicate a 95% confidence level of the linear regressions. (b) Observed and simulated dust means (dots) and standard deviations (error bars) vary with the SEUS regional-mean SPEI. Dash lines represent the linear regressions of the average dust concentrations with their slopes (Slope) and P-values (P-val) listed at the top-left corner.

The sensitivity of surface dust in response to the SEUS regional drought was also evaluated in the same way as Figure 2b. The results are displayed in Figure 8b. Similar to the fine dust responses to drought in the southeast, Barbados total dust also shows a decreasing tendency with lower SPEI. On average, dust at the Barbados site reduces by 1.85 $\mu\text{g}/\text{m}^3$ with a unite decrease of SPEI over the southeast region. This consolidates the conclusion that the weakened across-Atlantic transport of African dust is the reason causing the reduced fine dust in the SEUS as the Barbados site sits in the major transport pathway. GISS-E2-1-G simulations have a comparable sensitivity of 2.17 $\mu\text{g}/\text{m}^3$ (P-value= 0.13) despite its general overestimation, which makes it outperform the other three models which all have a much lower and less statistically significant sensitivity in response to SPEI changes.



Table 1. Evaluation metrics of four CMIP6 models in comparison with observations at the Barbados site. Metrics include correlation coefficient (R), mean bias (MB), normalized mean bias (NMB), root mean square error (RMSE), and slope.

Simulations	Drought Conditions	Observed Mean ($\mu\text{g}/\text{m}^3$)	Simulated Mean ($\mu\text{g}/\text{m}^3$)	R	MB ($\mu\text{g}/\text{m}^3$)	NMB (%)	RMSE ($\mu\text{g}/\text{m}^3$)	Slope
CNRM-ESM2-1	All months	25.51	2.38	0.20	-22.75	-82.98	24.75	0.03
	Severe Drought	23.53	2.33	0.17	-20.52	-80.49	21.62	0.04
GFDL-ESM4	All months	25.51	18.20	-0.26	-7.11	-25.93	15.94	-0.21
	Severe Drought	23.53	18.81	0.15	-4.49	-17.64	11.19	0.20
GISS-E2-1-G	All months	25.51	30.09	0.03	4.92	17.93	16.12	0.04
	Severe Drought	23.53	27.20	0.38	4.16	16.32	8.78	0.38
MRI-ESM2-0	All months	25.51	20.35	-0.12	-4.76	-17.38	14.91	-0.11
	Severe Drought	23.53	20.58	-0.05	-3.02	-11.84	12.90	-0.07

In conclusion, GISS-E2-1-G generally shows an overestimation of surface dust, while the other three models exhibit an underestimation with the highest underestimation found in the CNRM-ESM2-1 simulations. None of the four models are capable of capturing the dust variability using all the months, with GFDL-ESM4 and GISS-E2-1-G performing better if using the drought months only. GISS-E2-1-G can reproduce the dust-SPEI sensitivity much better than the other three models. It is noted that systematic bias should arise when comparing single-site observations with grid-mean predictions, which could presumably cause the between-model diversity as they have different spatial resolutions (Table S2). However, the dust-sensitivity evaluation should be less affected as its calculation depends more on relative changes, instead of absolute values.

4 Conclusions

We found an opposite response of surface fine dust to severe droughts between the western and southeastern CONUS, with an increase of $\sim 0.15 \mu\text{g}/\text{m}^3$ and a decrease of $\sim 0.5 \mu\text{g}/\text{m}^3$ per unit decrease of SPEI, respectively. Similar results were reached by the USDM-based drought conditions, with an average decrease of $0.23 \mu\text{g}/\text{m}^3$ over the SEUS relative to non-drought conditions. The dust and drought relationship over the west/southwest region has been investigated before due to its vicinity to the major dust source regions, and the increase of dust with drought is expected. As the southeast region is strongly influenced by long-range transport of African dust in the summer, we investigated how drought conditions in the SEUS affect the trans-Atlantic transport of African dust.

The elemental ratios are indicative of the dominance of African dust in the southeast region. The tendency of these ratios moving out of the normal range under severe droughts implies a reduced African dust input. The anomalies of satellite AOD and dust extinction coefficients suggest that both the transport and emissions of African dust are weaker during the southeast drought periods than normal. The composite analysis reveals that the weaker across-Atlantic dust transport is through the teleconnection patterns of the negative NAO. During the drought periods, a lower than normal and more northeastward displacement of the Bermuda High results in less dust being brought into the SEUS at low



362 levels from the Caribbean and Gulf of Mexico by its southwestward extensions. This can also be seen from a weaker
 363 and more shrinking CLLJ. Enhanced precipitation in Sahel associated with the northward shift of ITCZ leads to lower
 364 dust emissions therein.

365 At last, we evaluated four CMIP6 models with surface dust outputs. CNRM-ESM2-1 generally performs the worst
 366 with an up to 80% underestimation of the dust concentrations. While GFDL-ESM4 and MRI-ESM2-0 underpredict
 367 the dust level by 17% and 26%, respectively, GISS-E2-1-G shows an overestimation by 18%. All four models fail to
 368 reproduce the dust variability using data from all the months, with GFDL-ESM4 and GISS-E2-1-G models
 369 significantly improving their performance if only the drought months are used. Besides, GISS-E2-1-G outperforms
 370 other models in capturing the dust-SPEI sensitivity.

371 This study reveals how the local- or regional-scale drought conditions in the SEUS can be linked with the long-range
 372 transport and emission changes of African dust through teleconnections. Thus, in order to better predict how the local
 373 dust air quality will change in response to an increasing drought frequency in a warming climate (Cook et al., 2015),
 374 climate and Earth system models not only need to represent various physical processes associated with the entire dust
 375 cycle, but also should capture the abnormal atmospheric processes (e.g., circulation and precipitation) related to
 376 droughts. Evaluation of these models should use observations of dust-drought relationships not only in dust source
 377 regions but also in dust transported regions.

378 **Acknowledgments**

379 This research was supported by the NOAA's Atmospheric Chemistry, Carbon Cycle, and Climate (AC4) Program
 380 (NA19OAR4310177). The authors acknowledge NASA for providing the MODIS AOD and CALIPSO data, EPA
 381 and IMPROVE in making the dust observations. We thank individuals and groups for creating the USDM maps and
 382 the SPEI dataset. The authors also thank the modelling groups participating in the CMIP6 AerChemMIP project for
 383 making the surface dust outputs available.

384 **Data Availability**

385 The data used for this study can be downloaded through the links provided in Table S1 and Section 2.

386 **Competing interests**

387 The authors declare that they have no conflict of interest.

388 **Author contributions**

389 YW conceived the research idea. WL conducted the analysis. Both authors contributed to the preparation of the
 390 manuscript



391 References

- 392 Aarons, S. M., Arvin, L. J., Aciego, S. M., Riebe, C. S., Johnson, K. R., Blakowski, M. A., Koornneef, J. M., Hart,
 393 S. C., Barnes, M. E., Dove, N., Botthoff, J. K., Maltz, M., and Aronson, E. L.: Competing droughts affect dust
 394 delivery to Sierra Nevada, *Aeolian Res.*, 41, 100545, <https://doi.org/10.1016/j.aeolia.2019.100545>, 2019.
- 395 Achakulwisut, P., Shen, L., and Mickley, L. J.: What Controls Springtime Fine Dust Variability in the Western
 396 United States? Investigating the 2002–2015 Increase in Fine Dust in the U.S. Southwest, *J. Geophys. Res.*
 397 *Atmospheres*, 122, 12,449–12,467, <https://doi.org/10.1002/2017JD027208>, 2017.
- 398 Achakulwisut, P., Mickley, L. J., and Anenberg, S. C.: Drought-sensitivity of fine dust in the US Southwest:
 399 Implications for air quality and public health under future climate change, *Environ. Res. Lett.*, 13, 054025,
 400 <https://doi.org/10.1088/1748-9326/aabf20>, 2018.
- 401 Achakulwisut, P., Anenberg, S. C., Neumann, J. E., Penn, S. L., Weiss, N., Crimmins, A., Fann, N., Martinich, J.,
 402 Roman, H., and Mickley, L. J.: Effects of Increasing Aridity on Ambient Dust and Public Health in the U.S.
 403 Southwest Under Climate Change, *GeoHealth*, 3, 127–144, <https://doi.org/10.1029/2019GH000187>, 2019.
- 404 Alamirew, N. K., Todd, M. C., Ryder, C. L., Marsham, J. H., and Wang, Y.: The early summertime Saharan heat
 405 low: sensitivity of the radiation budget and atmospheric heating to water vapour and dust aerosol, *Atmospheric*
 406 *Chem. Phys.*, 18, 1241–1262, <https://doi.org/10.5194/acp-18-1241-2018>, 2018.
- 407 Aldhaif, A. M., Lopez, D. H., Dadashazar, H., and Sorooshian, A.: Sources, frequency, and chemical nature of dust
 408 events impacting the United States East Coast, *Atmos. Environ.*, 231, 117456,
 409 <https://doi.org/10.1016/j.atmosenv.2020.117456>, 2020.
- 410 Arcusa, S. H., McKay, N. P., Routson, C. C., and Munoz, S. E.: Dust-drought interactions over the last 15,000
 411 years: A network of lake sediment records from the San Juan Mountains, Colorado, *The Holocene*, 30, 559–574,
 412 <https://doi.org/10.1177/0959683619875192>, 2020.
- 413 Aryal, Y. N. and Evans, S.: Global Dust Variability Explained by Drought Sensitivity in CMIP6 Models, *J.*
 414 *Geophys. Res. Earth Surf.*, 126, e2021JF006073, <https://doi.org/10.1029/2021JF006073>, 2021.
- 415 Barnston, A. G. and Livezey, R. E.: Classification, Seasonality and Persistence of Low-Frequency Atmospheric
 416 Circulation Patterns, *Mon. Weather Rev.*, 115, 1083–1126, [https://doi.org/10.1175/1520-0493\(1987\)115<1083:CSAPOL>2.0.CO;2](https://doi.org/10.1175/1520-0493(1987)115<1083:CSAPOL>2.0.CO;2), 1987.
- 418 Borlina, C. S. and Rennó, N. O.: The Impact of a Severe Drought on Dust Lifting in California’s Owens Lake Area,
 419 *Sci. Rep.*, 7, 1784, <https://doi.org/10.1038/s41598-017-01829-7>, 2017.
- 420 Bou Karam, D., Flamant, C., Knippertz, P., Reitebuch, O., Pelon, J., Chong, M., and Dabas, A.: Dust emissions over
 421 the Sahel associated with the West African monsoon intertropical discontinuity region: A representative case-study,
 422 *Q. J. R. Meteorol. Soc.*, 134, 621–634, <https://doi.org/10.1002/qj.244>, 2008.
- 423 Brey, S., Pierce, J., Barnes, E., and Fischer, E.: Estimating the Spread in Future Fine Dust Concentrations in the
 424 Southwest United States, *J. Geophys. Res. Atmospheres*, 125, <https://doi.org/10.1029/2019JD031735>, 2020.
- 425 Carslaw, K. S., Boucher, O., Spracklen, D. V., Mann, G. W., Rae, J. G. L., Woodward, S., and Kulmala, M.: A
 426 review of natural aerosol interactions and feedbacks within the Earth system, *Atmospheric Chem. Phys.*, 10, 1701–
 427 1737, <https://doi.org/10.5194/acp-10-1701-2010>, 2010.
- 428 Chiapello, I., Moulin, C., and Prospero, J. M.: Understanding the long-term variability of African dust transport
 429 across the Atlantic as recorded in both Barbados surface concentrations and large-scale Total Ozone Mapping



- 430 Spectrometer (TOMS) optical thickness, *J. Geophys. Res. Atmospheres*, 110,
431 <https://doi.org/10.1029/2004JD005132>, 2005.
- 432 Cook, B. I., Ault, T. R., and Smerdon, J. E.: Unprecedented 21st century drought risk in the American Southwest
433 and Central Plains, *Sci. Adv.*, <https://doi.org/10.1126/sciadv.1400082>, 2015.
- 434 Cook, K. H.: Generation of the African Easterly Jet and Its Role in Determining West African Precipitation, *J.*
435 *Clim.*, 12, 1165–1184, [https://doi.org/10.1175/1520-0442\(1999\)012<1165:GOTAEJ>2.0.CO;2](https://doi.org/10.1175/1520-0442(1999)012<1165:GOTAEJ>2.0.CO;2), 1999.
- 436 Crooks, J. L., Cascio, W. E., Percy, M. S., Reyes, J., Neas, L. M., and Hilborn, E. D.: The Association between Dust
437 Storms and Daily Non-Accidental Mortality in the United States, 1993–2005, *Environ. Health Perspect.*, 124, 1735–
438 1743, <https://doi.org/10.1289/EHP216>, 2016.
- 439 Doherty, O. M., Riemer, N., and Hameed, S.: Saharan mineral dust transport into the Caribbean: Observed
440 atmospheric controls and trends, *J. Geophys. Res. Atmospheres*, 113, <https://doi.org/10.1029/2007JD009171>, 2008.
- 441 Dunne, J. P., Horowitz, L. W., Adcroft, A. J., Ginoux, P., Held, I. M., John, J. G., Krasting, J. P., Malyshev, S.,
442 Naik, V., Paulot, F., Shevliakova, E., Stock, C. A., Zadeh, N., Balaji, V., Blanton, C., Dunne, K. A., Dupuis, C.,
443 Durachta, J., Dussin, R., Gauthier, P. P. G., Griffies, S. M., Guo, H., Hallberg, R. W., Harrison, M., He, J., Hurlin,
444 W., McHugh, C., Menzel, R., Milly, P. C. D., Nikonov, S., Paynter, D. J., Ploshay, J., Radhakrishnan, A., Rand, K.,
445 Reichl, B. G., Robinson, T., Schwarzkopf, D. M., Sentman, L. T., Underwood, S., Vahlenkamp, H., Winton, M.,
446 Wittenberg, A. T., Wyman, B., Zeng, Y., and Zhao, M.: The GFDL Earth System Model Version 4.1 (GFDL-ESM
447 4.1): Overall Coupled Model Description and Simulation Characteristics, *J. Adv. Model. Earth Syst.*, 12,
448 e2019MS002015, <https://doi.org/10.1029/2019MS002015>, 2020.
- 449 Evan, A. T., Flamant, C., Gaetani, M., and Guichard, F.: The past, present and future of African dust, *Nature*, 531,
450 493–495, <https://doi.org/10.1038/nature17149>, 2016.
- 451 Flamant, C., Chaboureaud, J.-P., Parker, D. J., Taylor, C. M., Cammas, J.-P., Bock, O., Timouk, F., and Pelon, J.:
452 Airborne observations of the impact of a convective system on the planetary boundary layer thermodynamics and
453 aerosol distribution in the inter-tropical discontinuity region of the West African Monsoon, *Q. J. R. Meteorol. Soc.*,
454 133, 1175–1189, <https://doi.org/10.1002/qj.97>, 2007.
- 455 Folland, C. K., Knight, J., Linderholm, H. W., Fereday, D., Ineson, S., and Hurrell, J. W.: The Summer North
456 Atlantic Oscillation: Past, Present, and Future, *J. Clim.*, 22, 1082–1103, <https://doi.org/10.1175/2008JCLI2459.1>,
457 2009.
- 458 Francis, D., Fonseca, R., Nelli, N., Cuesta, J., Weston, M., Evan, A., and Temimi, M.: The Atmospheric Drivers of
459 the Major Saharan Dust Storm in June 2020, *Geophys. Res. Lett.*, 47, e2020GL090102,
460 <https://doi.org/10.1029/2020GL090102>, 2020.
- 461 Gonzalez, M. E., Garfield, J. G., Corral, A. F., Edwards, E.-L., Zeider, K., and Sorooshian, A.: Extreme Aerosol
462 Events at Mesa Verde, Colorado: Implications for Air Quality Management, *Atmosphere*, 12, 1140,
463 <https://doi.org/10.3390/atmos12091140>, 2021.
- 464 Hand, J. L., Schichtel, B. A., Pitchford, M., Malm, W. C., and Frank, N. H.: Seasonal composition of remote and
465 urban fine particulate matter in the United States, *J. Geophys. Res. Atmospheres*, 117,
466 <https://doi.org/10.1029/2011JD017122>, 2012.
- 467 Hand, J. L., Gill, T. E., and Schichtel, B. A.: Spatial and seasonal variability in fine mineral dust and coarse aerosol
468 mass at remote sites across the United States, *J. Geophys. Res. Atmospheres*, 122, 3080–3097,
469 <https://doi.org/10.1002/2016JD026290>, 2017.



- 470 Hurrell, J. W.: Decadal Trends in the North Atlantic Oscillation: Regional Temperatures and Precipitation, *Science*,
471 269, 676–679, 1995.
- 472 Jones, C., Mahowald, N., and Luo, C.: The Role of Easterly Waves on African Desert Dust Transport, *J. Clim.*, 16,
473 3617–3628, [https://doi.org/10.1175/1520-0442\(2003\)016<3617:TROEWO>2.0.CO;2](https://doi.org/10.1175/1520-0442(2003)016<3617:TROEWO>2.0.CO;2), 2003.
- 474 Jones, P. D., Jonsson, T., and Wheeler, D.: Extension to the North Atlantic oscillation using early instrumental
475 pressure observations from Gibraltar and south-west Iceland, *Int. J. Climatol.*, 17, 1433–1450,
476 [https://doi.org/10.1002/\(SICI\)1097-0088\(19971115\)17:13<1433::AID-JOC203>3.0.CO;2-P](https://doi.org/10.1002/(SICI)1097-0088(19971115)17:13<1433::AID-JOC203>3.0.CO;2-P), 1997.
- 477 Karanasiou, A., Moreno, N., Moreno, T., Viana, M., de Leeuw, F., and Querol, X.: Health effects from Sahara dust
478 episodes in Europe: Literature review and research gaps, *Environ. Int.*, 47, 107–114,
479 <https://doi.org/10.1016/j.envint.2012.06.012>, 2012.
- 480 Kelley, M., Schmidt, G. A., Nazarenko, L. S., Bauer, S. E., Ruedy, R., Russell, G. L., Ackerman, A. S., Aleinov, I.,
481 Bauer, M., Bleck, R., Canuto, V., Cesana, G., Cheng, Y., Clune, T. L., Cook, B. I., Cruz, C. A., Del Genio, A. D.,
482 Elsaesser, G. S., Faluvegi, G., Kiang, N. Y., Kim, D., Lacis, A. A., Leboissetier, A., LeGrande, A. N., Lo, K. K.,
483 Marshall, J., Matthews, E. E., McDermid, S., Mezzuman, K., Miller, R. L., Murray, L. T., Oinas, V., Orbe, C.,
484 García-Pando, C. P., Perlwitz, J. P., Puma, M. J., Rind, D., Romanou, A., Shindell, D. T., Sun, S., Tausnev, N.,
485 Tsigaridis, K., Tselioudis, G., Weng, E., Wu, J., and Yao, M.-S.: GISS-E2.1: Configurations and Climatology, *J.*
486 *Adv. Model. Earth Syst.*, 12, e2019MS002025, <https://doi.org/10.1029/2019MS002025>, 2020.
- 487 Kelly, P. and Mapes, B.: Zonal mean wind, the Indian monsoon, and July drying in the western Atlantic subtropics,
488 *J. Geophys. Res. Atmospheres*, 116, <https://doi.org/10.1029/2010JD015405>, 2011.
- 489 Kim, D., Chin, M., Cruz, C. A., Tong, D., and Yu, H.: Spring Dust in Western North America and Its Interannual
490 Variability—Understanding the Role of Local and Transported Dust, *J. Geophys. Res. Atmospheres*, 126,
491 e2021JD035383, <https://doi.org/10.1029/2021JD035383>, 2021.
- 492 Knippertz, P. and Todd, M. C.: The central west Saharan dust hot spot and its relation to African easterly waves and
493 extratropical disturbances, *J. Geophys. Res. Atmospheres*, 115, <https://doi.org/10.1029/2009JD012819>, 2010.
- 494 Li, W., Li, L., Fu, R., Deng, Y., and Wang, H.: Changes to the North Atlantic Subtropical High and Its Role in the
495 Intensification of Summer Rainfall Variability in the Southeastern United States, *J. Clim.*, 24, 1499–1506,
496 <https://doi.org/10.1175/2010JCLI3829.1>, 2011.
- 497 Li, W., Wang, Y., Flynn, J., Griffin, R. J., Guo, F., and Schnell, J. L.: Spatial Variation of Surface O₃ Responses to
498 Drought Over the Contiguous United States During Summertime: Role of Precursor Emissions and Ozone
499 Chemistry, *J. Geophys. Res. Atmospheres*, 127, e2021JD035607, <https://doi.org/10.1029/2021JD035607>, 2022.
- 500 Linderholm, H. W., Folland, C. K., and Walther, A.: A multicentury perspective on the summer North Atlantic
501 Oscillation (SNAO) and drought in the eastern Atlantic Region, *J. Quat. Sci.*, 24, 415–425,
502 <https://doi.org/10.1002/jqs.1261>, 2009.
- 503 Liu, C., Liao, X., Qiu, J., Yang, Y., Feng, X., Allan, R. P., Cao, N., Long, J., and Xu, J.: Observed variability of
504 intertropical convergence zone over 1998–2018, *Environ. Res. Lett.*, 15, 104011, <https://doi.org/10.1088/1748-9326/aba033>, 2020.
- 506 Middleton, N. J.: Desert dust hazards: A global review, *Aeolian Res.*, 24, 53–63,
507 <https://doi.org/10.1016/j.aeolia.2016.12.001>, 2017.
- 508 Moulin, C. and Chiapello, I.: Evidence of the control of summer atmospheric transport of African dust over the
509 Atlantic by Sahel sources from TOMS satellites (1979–2000), *Geophys. Res. Lett.*, 31,
510 <https://doi.org/10.1029/2003GL018931>, 2004.



- 511 Payra, S., Gupta, P., Bhatla, R., El Amraoui, L., and Verma, S.: Temporal and spatial variability in aerosol optical
 512 depth (550 nm) over four major cities of India using data from MODIS onboard the Terra and Aqua satellites, Arab.
 513 J. Geosci., 14, 1256, <https://doi.org/10.1007/s12517-021-07455-y>, 2021.
- 514 Perry, K. D., Cahill, T. A., Eldred, R. A., Dutcher, D. D., and Gill, T. E.: Long-range transport of North African dust
 515 to the eastern United States, J. Geophys. Res. Atmospheres, 102, 11225–11238, <https://doi.org/10.1029/97JD00260>,
 516 1997.
- 517 Prospero, J. M. and Mayol-Bracero, O. L.: Understanding the Transport and Impact of African Dust on the
 518 Caribbean Basin, Bull. Am. Meteorol. Soc., 94, 1329–1337, <https://doi.org/10.1175/BAMS-D-12-00142.1>, 2013.
- 519 Prospero, J. M. and Nees, R. T.: Impact of the North African drought and El Niño on mineral dust in the Barbados
 520 trade winds, Nature, 320, 735–738, <https://doi.org/10.1038/320735a0>, 1986.
- 521 Prospero, J. M., Landing, W. M., and Schulz, M.: African dust deposition to Florida: Temporal and spatial
 522 variability and comparisons to models, J. Geophys. Res. Atmospheres, 115, <https://doi.org/10.1029/2009JD012773>,
 523 2010.
- 524 Pu, B. and Ginoux, P.: Climatic factors contributing to long-term variations in surface fine dust concentration in the
 525 United States, Atmospheric Chem. Phys., 18, 4201–4215, <https://doi.org/10.5194/acp-18-4201-2018>, 2018.
- 526 Pu, B. and Jin, Q.: A Record-Breaking Trans-Atlantic African Dust Plume Associated with Atmospheric Circulation
 527 Extremes in June 2020, Bull. Am. Meteorol. Soc., 102, E1340–E1356, <https://doi.org/10.1175/BAMS-D-21-0014.1>,
 528 2021.
- 529 Ridley, D. A., Heald, C. L., and Ford, B.: North African dust export and deposition: A satellite and model
 530 perspective, J. Geophys. Res. Atmospheres, 117, <https://doi.org/10.1029/2011JD016794>, 2012.
- 531 Sassen, K.: Indirect climate forcing over the western US from Asian dust storms, Geophys. Res. Lett., 29, 103-1-
 532 103-4, <https://doi.org/10.1029/2001GL014051>, 2002.
- 533 Schnell, J. L., Holmes, C. D., Jangam, A., and Prather, M. J.: Skill in forecasting extreme ozone pollution episodes
 534 with a global atmospheric chemistry model, Atmospheric Chem. Phys., 14, 7721–7739, <https://doi.org/10.5194/acp-14-7721-2014>, 2014.
- 536 Séférian, R., Nabat, P., Michou, M., Saint-Martin, D., Voldoire, A., Colin, J., Decharme, B., Delire, C., Berthet, S.,
 537 Chevallier, M., Sénéci, S., Franchisteguy, L., Vial, J., Mallet, M., Joetzjer, E., Geoffroy, O., Guérémy, J.-F., Moine,
 538 M.-P., Msadek, R., Ribes, A., Rocher, M., Roehrig, R., Salas-y-Méla, D., Sanchez, E., Terray, L., Valcke, S.,
 539 Waldman, R., Aumont, O., Bopp, L., Deshayes, J., Éthé, C., and Madec, G.: Evaluation of CNRM Earth System
 540 Model, CNRM-ESM2-1: Role of Earth System Processes in Present-Day and Future Climate, J. Adv. Model. Earth
 541 Syst., 11, 4182–4227, <https://doi.org/10.1029/2019MS001791>, 2019.
- 542 Sheen, K. L., Smith, D. M., Dunstone, N. J., Eade, R., Rowell, D. P., and Vellinga, M.: Skilful prediction of Sahel
 543 summer rainfall on inter-annual and multi-year timescales, Nat. Commun., 8, 14966,
 544 <https://doi.org/10.1038/ncomms14966>, 2017.
- 545 Svoboda, M., LeComte, D., Hayes, M., Heim, R., Gleason, K., Angel, J., Rippey, B., Tinker, R., Palecki, M.,
 546 Stooksbury, D., Miskus, D., and Stephens, S.: The drought monitor, Bull. Am. Meteorol. Soc., 83, 1181–1190,
 547 <https://doi.org/10.1175/1520-0477-83.8.1181>, 2002.
- 548 Tegen, I., Lacis, A. A., and Fung, I.: The influence on climate forcing of mineral aerosols from disturbed soils,
 549 Nature, 380, 419–422, <https://doi.org/10.1038/380419a0>, 1996.



- 550 Tong, D. Q., Wang, J. X. L., Gill, T. E., Lei, H., and Wang, B.: Intensified dust storm activity and Valley fever
 551 infection in the southwestern United States, *Geophys. Res. Lett.*, 44, 4304–4312,
 552 <https://doi.org/10.1002/2017GL073524>, 2017.
- 553 VanCuren, R. A. and Cahill, T. A.: Asian aerosols in North America: Frequency and concentration of fine dust, *J.*
 554 *Geophys. Res. Atmospheres*, 107, AAC 19-1-AAC 19-16, <https://doi.org/10.1029/2002JD002204>, 2002.
- 555 Visbeck, M. H., Hurrell, J. W., Polvani, L., and Cullen, H. M.: The North Atlantic Oscillation: Past, present, and
 556 future, *Proc. Natl. Acad. Sci.*, 98, 12876–12877, <https://doi.org/10.1073/pnas.231391598>, 2001.
- 557 Wang, C.: Variability of the Caribbean Low-Level Jet and its relations to climate, *Clim. Dyn.*, 29, 411–422,
 558 <https://doi.org/10.1007/s00382-007-0243-z>, 2007.
- 559 Wang, Y., Xie, Y., Dong, W., Ming, Y., Wang, J., and Shen, L.: Adverse effects of increasing drought on air quality
 560 via natural processes, *Atmospheric Chem. Phys.*, 17, 12827–12843, <https://doi.org/10.5194/acp-17-12827-2017>,
 561 2017.
- 562 Yu, H., Tan, Q., Zhou, L., Zhou, Y., Bian, H., Chin, M., Ryder, C. L., Levy, R. C., Pradhan, Y., Shi, Y., Song, Q.,
 563 Zhang, Z., Colarco, P. R., Kim, D., Remer, L. A., Yuan, T., Mayol-Bracero, O., and Holben, B. N.: Observation and
 564 modeling of the historic “Godzilla” African dust intrusion into the Caribbean Basin and the southern US in June
 565 2020, *Atmospheric Chem. Phys.*, 21, 12359–12383, <https://doi.org/10.5194/acp-21-12359-2021>, 2021.
- 566 Yuan, T., Yu, H., Chin, M., and Remer, L.: Future Decline of African Dust: Insights from the Recent Past and
 567 Paleo-records, *ArXiv180407188 Phys.*, 2018.
- 568 Yukimoto, S., Kawai, H., Koshiro, T., Oshima, N., Yoshida, K., Urakawa, S., Tsujino, H., Deushi, M., Tanaka, T.,
 569 Hosaka, M., Yabu, S., Yoshimura, H., Shindo, E., Mizuta, R., Obata, A., Adachi, Y., and Ishii, M.: The
 570 Meteorological Research Institute Earth System Model Version 2.0, MRI-ESM2.0: Description and Basic
 571 Evaluation of the Physical Component, *J. Meteorol. Soc. Jpn. Ser II*, 97, 931–965,
 572 <https://doi.org/10.2151/jmsj.2019-051>, 2019.
- 573 Zhao, A., Ryder, C. L., and Wilcox, L. J.: How well do the CMIP6 models simulate dust aerosols?, *Atmospheric*
 574 *Chem. Phys. Discuss.*, 1–32, <https://doi.org/10.5194/acp-2021-578>, 2021.
- 575 Zuidema, P., Alvarez, C., Kramer, S. J., Custals, L., Izaguirre, M., Sealy, P., Prospero, J. M., and Blades, E.: Is
 576 Summer African Dust Arriving Earlier to Barbados? The Updated Long-Term In Situ Dust Mass Concentration
 577 Time Series from Ragged Point, Barbados, and Miami, Florida, *Bull. Am. Meteorol. Soc.*, 100, 1981–1986,
 578 <https://doi.org/10.1175/BAMS-D-18-0083.1>, 2019.

579